Infrared Spectroscopic Evidence for Inversion Ring Opening in Ethylene Oxide Polymerization

Masaaki Yokoyama,[1a] Hiroshi Ochi,[1a] Hiroyuki Tadokoro,*[1a] and Charles C. Price[1b]

Department of Polymer Science, Faculty of Science, Osaka University, Toyonaka, Osaka, 560 Japan, and Department of Chemistry, University of Pennsylvania, Philadelphia, Pennsylvania. *Received June 19, 1972*

ABSTRACT: Infrared spectra of poly(*cis*-dideuterioethylene oxide) and poly(*trans*-dideuterioethylene oxide) polymerized by cationic, anionic, and coordination catalysts were studied in connection with the way of ring opening in the polymerization. The polarized spectra of oriented films as well as the spectra in the molten state and in solutions show distinct differences depending only on the configuration of the monomer. The normal vibrations were calculated by transferring force constants of the valence force type adjusted by repetitions of the least-squares method for poly(ethylene oxide) and poly(ethylene-d_4 oxide). The spectral differences especially in the 1500–1100-cm^{-1} region are reasonably expected to be due to vibrational modes localized within the monomeric unit. The calculations were made for the following five models: threo diisotactic (two optical antipodes), threo disyndiotactic, erythro diisotactic, and erythro disyndiotactic. By comparing the observed spectra and the calculated results, it was found that the cis and trans polymers have the threo and erythro configurations, respectively. This experimental fact indicates inversion ring-opening polymerization.

In a previous paper[2] it was reported that poly(*cis*-dideuterioethylene oxide) (*cis*-PEO-d_2) and poly(*trans*-dideuterioethylene oxide) (*trans*-PEO-d_2) polymerized by cationic, anionic, and coordination catalysts showed different infrared spectra depending only on the configuration of the monomer. In this paper we wish to report evidence for inversion ring opening based on a comparison between the infrared spectra of the polymers obtained from the two isomeric monomers and the results of the normal-coordinate treatment for the possible polymer models.

Samples and Spectral Measurements

In this study, the three kinds of polymers given in Table I were used. The films for infrared measurements were made by rolling the powder samples or by casting from chloroform solutions. The infrared absorption spectra were taken by using a Japan Spectroscopic Co. Model DS-402G double-beam grating spectrophotometer with a AgCl polarizer set in front of the detector. Since the preparation of oriented films with sizes sufficient for measurements by the usual infrared spectrophotometer were difficult for samples II and III, the polarized spectra of these samples were measured by using the microspectroscopic attachment.

The polarized infrared spectra of samples I, II, and III are reproduced in Figure 1. The solid and broken curves represent absorptions obtained with polarized radiation with electric vectors perpendicular and parallel to the orientation direction, respectively. The figures adjacent to the curves represent the specimen thickness in microns measured with a bench thickness gauge. The frequencies, the relative intensities, and the polarization properties of the absorption bands are summarized in Table II. Figures 2 and 3 are spectra of the two types of samples in molten states (at about 80°) and in benzene solutions, respectively. The spectra in deuterated chloroform solutions give similar data.

Molecular Models

If the inversion mechanism is the case, the cis and trans monomers should give polymers having threo monomeric units (A or B given below by Fischer projections) and erythro monomeric units (C), respectively. On the contrary, if the inversion does not occur, the relation should be opposite.

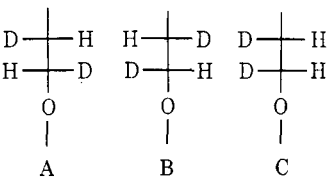

A B C

Consequently, the configuration of the monomeric unit of the polymer obtained from either of the cis or trans monomer must be threo or erythro, but the relation between the neighboring monomeric units in polymers, that is, isotactic or syndiotactic, may be completely random. If the diisotactic (dit) and disyndiotactic (dst) polymers consisting of the threo or erythro monomeric units are considered as the limiting ideal cases, only the following five models are possible: threo-diisotactic model A, threo-diisotactic model B, threo disyndiotactic, erythro diisotactic, and erythro disyndiotactic.

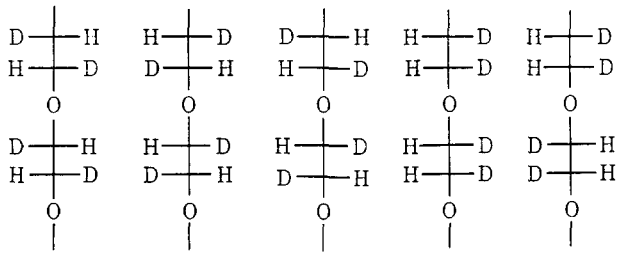

threo-dit A threo-dit B threo dst erythro dit erythro dst

The molecular conformation of polyethylene oxide (PEO) in the crystalline state is a helix containing seven chemical units and two turns in the fiber identity period 19.3 Å, and consists of sequences of nearly trans, trans, and gauche forms.[3] The spectroscopic unit cell contains 7 monomeric units and 2 turns for the diisotactic models and 14 monomeric units and 4 turns for the disyndiotactic models, twice the diisotactic case. The threo-diisotactic models A and B are optical

(1) (a) Osaka University; (b) University of Pennsylvania.
(2) C. C. Price and R. Spector, *J. Amer. Chem. Soc.*, **88**, 4171 (1966).
(3) H. Tadokoro, Y. Chatani, T. Yoshihara, S. Tahara, and S. Murahashi, *Makromol. Chem.*, 73, 109 (1964).

TABLE I
POLY(DIDEUTERIOETHYLENE OXIDE) SAMPLES USED FOR INFRARED MEASUREMENTS[a]

Sample	Starting monomer	Catalyst	Intrinsic viscosity	Av mol wt[b]
I	Trans	$AlEt_3$–H_2O	0.30	16,000
II	Trans	$FeCl_3$–PO	1.34	214,000
III	Cis	$ZnEt_2$–H_2O	0.65	60,000

[a] These samples are the same ones already reported in ref 2. Viscosity was measured in benzene solutions at 25°. [b] $[\eta] = (9.8 \times 10^{-4})M^{0.59}$.

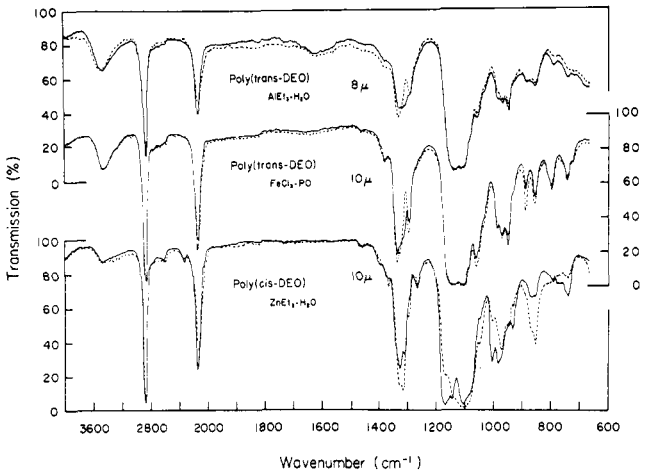

Figure 1. Polarized infrared spectra of poly(*trans*-dideuterioethylene oxide) and poly(*cis*-dideuterioethylene oxide): (——) electric vector perpendicular to elongation, (– – –) electric vector parallel to elongation.

antipodes of each other, and these two models give different conformations with respect to deuterium, if the helix of the same sense is considered, right handed or left handed. In the right-handed helix the threo monomeric units A and B have the conformations expressed by Newman projections I and II viewed along the gauche C–C bond, respectively. In cases I and II, the oxygen atoms are nearly trans to both deuterium and both hydrogen atoms, respectively, and there is a twofold rotation axis passing through the midpoint of the C–C bond. The erythro unit C has the conformation of the Newman projection III, in which one oxygen atom is nearly trans to a hydrogen atom, and the other oxygen atom is nearly trans to a deuterium. In this case, therefore, no twofold

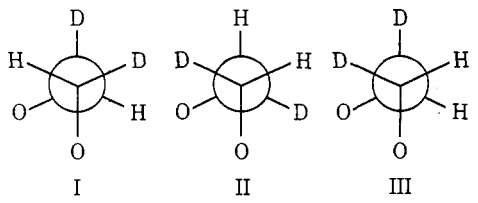

rotation axis exists on the midpoint of the C–C bond. In the case of the threo-diisotactic models, there are two types of twofold rotation axes, which intersect the helix axis perpendicularly and pass through the oxygen atoms and the centers of the C–C bonds, respectively, just as in the case of PEO. In the threo-disyndiotactic model, there are twofold axes passing only through the centers of the C–C bonds. On the other hand, the erythro-disyndiotactic model has twofold

TABLE II
INFRARED SPECTRA OF POLY(*cis*-DIDEUTERIOETHYLENE OXIDE) AND POLY(*trans*-DIDEUTERIOETHYLENE OXIDE)

Poly(*cis*-dideuterioethylene oxide)			Poly(*trans*-dideuterioethylene oxide)		
Frequency, cm^{-1}	Dichroism	Intensity	Frequency, cm^{-1}	Dichroism	Intensity
2874	⊥	s	2874	⊥	s
2870	∥	s	2859	∥	s
2618	⊥	vvw	2755	∥	vvw
2580	∥	vvw	2664	∥	vvw
2149	⊥	m	2578	∥	vvw
2133	∥	m	2150	⊥	m
1397	⊥	vw	2126	∥	m
1368	∥	w	1376	⊥	w
1341	⊥	sh	1342	∥	sh
1326	⊥, ∥	s	1330	∥	s
1316	∥	s	1322	∥	sh
1310	⊥	m	1319	⊥	sh
1298	∥	sh	1311	⊥	sh
1268	⊥	w	1294	∥	m
1169	⊥	vs	1289	⊥	m
1167	∥	s	1147	⊥	vs
1144	⊥	vs	1135	⊥	vs
1139	∥	sh	1120	∥	sh
1105	⊥, ∥	vs	1104	⊥	vs
1087	∥	sh	1084	⊥	sh
1050	∥	sh	1057	∥	m
1004	⊥	m	1032	∥	sh
1003	∥	w	986	⊥	m
983	⊥	m	981	∥	m
971	∥	m	967	∥	m
945	∥	w	946	⊥	m
933	⊥	w	927	⊥	sh
931	∥	vw	884	∥	m
867	⊥	w	855	∥	w
862	∥	sh	852	⊥	w
853	∥	m	795	⊥	sh
791	⊥	vw	791	∥	w
741	⊥	w	735	⊥	w
			717	⊥	vvw

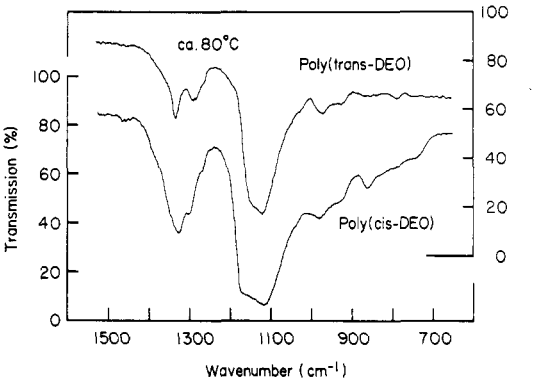

Figure 2. Infrared spectra of molten state (80°).

axes only on the oxygen atoms. Thus, all three threo polymer models and the erythro-disyndiotactic model have dihedral symmetry, while the erythro-diisotactic model has only cyclic symmetry.

The polarized infrared spectra of the two types of polymers show distinct differences as indicated by arrows in Figure 4, which reproduce the 1500–700-cm^{-1} region for the convenience of comparison. The strong 1169-cm^{-1} band characteristic of the cis polymer appears also in the molten

TABLE III
CHARACTER TABLE, NUMBERS OF NORMAL MODES, AND SELECTION RULES FOR THE FIVE IDEAL MODELS[a]

(1) Threo-diisotactic models A and B ($\omega = 4\pi/7$)								
$D(4\pi/7)$	E	$2C^1$	$2C^2$	$2C^3$	$7C_2$	N	Ir	Raman
A_1	1	1	1	1	1	10	F	A
A_2	1	1	1	1	−1	$11 - 2(T_\parallel, R_\parallel)$	$A(\parallel)$	F
E_1	2	$2\cos\omega$	$2\cos 2\omega$	$2\cos 3\omega$	0	$[21 - 1(T_\perp)] \times 2$	$A(\perp)$	A
E_2	2	$2\cos 2\omega$	$2\cos 4\omega$	$2\cos 6\omega$	0	21×2	F	A
E_3	2	$2\cos 3\omega$	$2\cos 6\omega$	$2\cos 9\omega$	0	21×2	F	F

(2) Threo-disyndiotactic model ($\omega = 8\pi/7$)								
$D(8\pi/7)$	E	$2C^1$	$2C^2$	$2C^3$	$7C_2$	N	Ir	Raman
A_1	1	1	1	1	1	21	F	A
A_2	1	1	1	1	−1	$21 - 2(T_\parallel, R_\parallel)$	$A(\parallel)$	F
E_1	2	$2\cos\omega$	$2\cos 2\omega$	$2\cos 3\omega$	0	$[42 - 1(T_\perp)] \times 2$	$A(\perp)$	A
E_2	2	$2\cos 2\omega$	$2\cos 4\omega$	$2\cos 6\omega$	0	42×2	F	A
E_3	2	$2\cos 3\omega$	$2\cos 6\omega$	$2\cos 9\omega$	0	42×2	F	F

(3) Erythro-diisotactic model [$\epsilon = \exp(4\pi i/7)$]										
$C(4\pi/7)$	E	C^1	C^2	C^3	C^4	C^5	C^6	N	Ir	Raman
A	1	1	1	1	1	1	1	$21 - 2(T_\parallel, R_\parallel)$	$A(\parallel)$	A
E_1	1	ϵ	ϵ^2	ϵ^3	ϵ^{-3}	ϵ^{-2}	ϵ^{-1}	$21 - 1(T_\perp)$	$A(\perp)$	A
	1	ϵ^{-1}	ϵ^{-2}	ϵ^{-3}	ϵ^3	ϵ^2	ϵ	$21 - 1(T_\perp)$		
E_2	1	ϵ^2	ϵ^{-3}	ϵ^{-1}	ϵ	ϵ^3	ϵ^{-2}	21	F	A
	1	ϵ^{-2}	ϵ^3	ϵ	ϵ^{-1}	ϵ^{-3}	ϵ^2	21		
E_3	1	ϵ^3	ϵ^{-1}	ϵ^2	ϵ^{-2}	ϵ	ϵ^{-3}	21	F	F
	1	ϵ^{-3}	ϵ	ϵ^{-2}	ϵ^2	ϵ^{-1}	ϵ^3	21		

(4) Erythro-disyndiotactic model ($\omega = 8\pi/7$)								
$D(8\pi/7)$	E	$2C^1$	$2C^2$	$2C^3$	$7C_2$	N	Ir	Raman
A_1	1	1	1	1	1	20	F	A
A_2	1	1	1	1	−1	$22 - 2(T_\parallel, R_\parallel)$	$A(\parallel)$	F
E_1	2	$2\cos\omega$	$2\cos 2\omega$	$2\cos 3\omega$	0	$[42 - 1(T_\perp)] \times 2$	$A(\perp)$	A
E_2	2	$2\cos 2\omega$	$2\cos 4\omega$	$2\cos 6\omega$	0	42×2	F	A
E_3	2	$2\cos 3\omega$	$2\cos 6\omega$	$2\cos 9\omega$	0	42×2	F	F

[a] The symmetry operation C^k ($k = 1, 2, \ldots, 6$) is a rotation of angle $k\omega$ about the axis of the helix followed by a transition along the axis of $k/7$ of the unit cell length. N is the number of total normal modes under each symmetry species. $R_\parallel$ is pure rotation about the axis. A = active, F = forbidden. $\perp$ or $\parallel$ indicates the oscillating electric vector parallel or perpendicular, respectively, to the helix axis. $T_\perp$ and $T_\parallel$ represent pure translations.

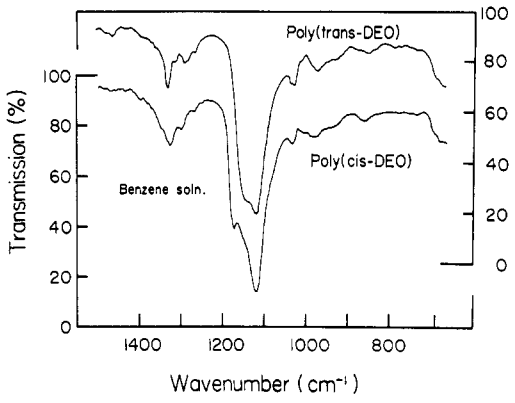

Figure 3. Infrared spectra of benzene solutions.

state and in benzene or deuterated chloroform solution (Figures 2 and 3). These facts suggest the possibility that the spectra of these two polymers, especially in the 1500–1100-cm^{-1} region, reflect the characteristic features associated with the vibrational modes localized within the unit. Consequently, it is reasonable to expect to identify the threo and erythro configurations by using spectral differences in this region.

From this point of view the comparison between the infrared spectra and the results of the normal coordinate treatment for the aforementioned five models are sufficient for the present purpose. This situation is supported further by the results of frequency-phase difference curves as will be discussed later.

Normal Coordinate Treatments

The results of the factor group analyses for the five ideal models are given in Table III. Here it may be noticed that the number of normal vibrations belonging to the A_1 or A_2 species is different for the threo- and erythro-disyndiotactic polymer models in spite of the fact that they belong to the same dihedral group, $D(8\pi/7)$. As discussed above, the actual polymers are expected to have either the erythro or threo configuration, but the relation between the neighboring monomeric units, that is, isotactic or syndiotactic, is completely random. Therefore, the selection rules should not hold strictly, but the general features of the spectra, especially in the 1500–1100-cm^{-1} region, will be interpreted reasonably based upon the results of the normal coordinate treatments. In order to obtain the most reliable force constants, those of the valence force type were at first transferred from aliphatic ethers,[4] and then were adjusted by repetitions of the least-squares method so as to give good agreement between the

(4) R. G. Snyder and G. Zerbi, *Spectrochim. Acta, Part A*, **23**, 391 (1967).

TABLE IV
FORCE CONSTANTS

Force constants	Group[a]	Poly(ethylene oxide)	Aliphatic ethers[4]
	Stretch, mdyn/Å		
K_r	C–CH_2–O (C–H)	4.626	4.626
K_D	C–O (C–O)	4.973	5.090
K_R	C–C (C–C)	5.131	4.261
	Bend, (mdyn Å)/rad		
H_δ	C–CH_2–O (∠HCH)	0.462	0.471
H_ω	C–CH_2–O (∠HCO)	0.868	0.901
H_ϕ	C–CH_2–O (∠HCC)	0.730	0.752
H_θ	C–O–C (∠COC)	1.564	1.313
H_Θ	C–C–O (∠CCO)	1.527	1.182
	Torsion, (mdyn Å)/rad		
H_T	C–C–O–C (C–O)	0.092	0.026
H_τ	O–C–C–O (C–C)	0.110	0.024
	Stretch–Stretch, mdyn/Å		
F_r	C–CH_2–O (C–H, C–H) [C]	−0.046	−0.046
F_D	C–O–C (C–O, C–O) [O]	0.054	0.288
F_{RD}	C–C–O (C–C, C–O) [C]	0.453	0.101
	Stretch–Bend, mdyn/rad		
$F_{D\omega}$	C–CH–O (C–O, ∠HCO) [C–O]	0.628	0.387
$F_{R\phi}$	C–CH–O (C–C, ∠HCC) [C–C]	0.056	0.478
$F_{D\theta}$	C–O–C (C–O, ∠COC) [C–O]	0.217	0.487
$F_{D\Theta}$	C–C–O (C–O, ∠CCO) [C–O]	0.779	0.618
$F_{R\Theta}$	C–C–O (C–C, ∠CCO) [C–C]	0.896	0.403
	Bend–Bend, mdyn/(rad)^2		
F_ω	C–CH_2–O (∠HCO, ∠HCO) [C–O]	0.004	−0.005
F_ϕ	C–CH_2–O (∠HCC, ∠HCC) [C–C]	0.039	0.105
$F_{\omega\phi}$	C–CH_2–O (∠HCC, ∠HCO) [C–H]	0.098	0.115
$F_{\omega\Theta}$	C–CH_2–O (∠HCO, ∠CCO) [C–O]	0.227	−0.031
$F_{\phi\Theta}$	C–CH_2–O (∠HCC, ∠CCO) [C–C]	−0.006	−0.031
f_{ϕ^g}	HC–CH (G) (∠HCC, ∠HCC) [C–C]	−0.013	0.004
f_{ϕ^t}	HC–CH (T) (∠HCC, ∠HCC) [C–C]	0.104	0.121
$f_{\omega\theta^g}$	HC–OC (G) (∠HCO, ∠COC) [C–O]	0.100	0.004
$f_{\phi\Theta^g}$	HC–CO (G) (∠HCC, ∠CCO) [C–C]	−0.243	−0.113
$f_{\phi\Theta^t}$	HC–CO (T) (∠HCC, ∠CCO)[C–C]	0.037	0.028
$f_{\theta\Theta^t}$	CO–CC (T) (∠COC, ∠OCC) [C–O]	−0.091	−0.011
f_{Θ^g}	OC–CO (G) (∠OCC, ∠CCO) [C–C]	−0.038	0.011

[a] The coordinate(s) involved and the atoms common to the interacting coordinates are shown in parentheses and brackets, respectively. HC–CH (G) indicates that the two hydrogen atoms in question are in the gauche relation (T, trans).

observed and calculated frequencies for PEO and PEO-d_4.[5] The molecular parameters assumed in the present work are as follows: (1) the interatomic distances C–H (D) = 1.09, C–O = 1.43, and C–C = 1.54 Å; (2) all the bond angles = 109°28′; and (3) the internal rotation angles τ(CCOC) = 188°15′ and τ(OCCO) = 64°58′.[3,5] The coordinates used are given in the Appendix.

The values of the most plausible set of force constants are given in Table IV, compared with those of aliphatic ethers. The results for PEO and PEO-d_4 are given in Table V and Figure 5. The maximum and average deviations are 1.96 and 0.53% for PEO and 3.16 and 0.92% for PEO-d_4, respectively. The potential energy distributions of several bands are different from those of the previous paper.[5] These may be due to the difference in the types of potential field, and the present result is considered to be more reasonable. The vibrational modes having appreciable deviations appear in the low-frequency region (skeletal bending and torsional

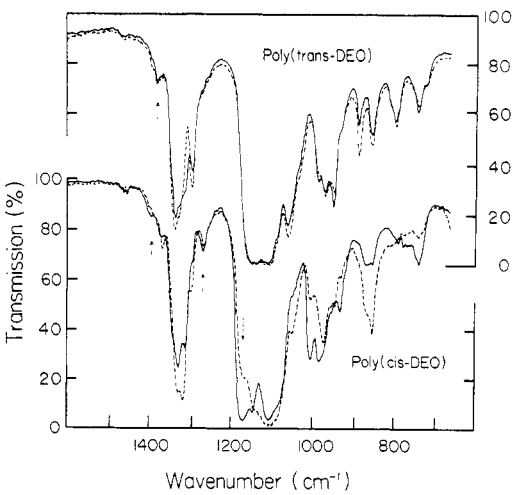

Figure 4. Polarized infrared spectra of poly(*trans*-dideuterioethylene oxide) and poly(*cis*-dideuterioethylene oxide) in the 1500–700-cm^{-1} region: (——) electric vector perpendicular to elongation, (– – –) electric vector parallel to elongation.

(5) T. Yoshihara, H. Tadokoro, and S. Murahashi, *J. Chem. Phys.*, 41, 2902 (1964).

TABLE V
OBSERVED AND CALCULATED FREQUENCIES (CM^{-1}) AND POTENTIAL ENERGY DISTRIBUTIONS FOR POLY(ETHYLENE OXIDE) AND POLY(ETHYLENE-d_4 OXIDE)

Species	Obsd frequency: Infrared	Obsd frequency: Raman	Calcd frequency	Assignment (Potential energy distribution, %)[a]
		(a) Poly(ethylene oxide)		
A_1		1483 (s)	1482	$\delta(CH_2)_s(75) + \nu(CC)(13)$
		1398 (vw)	1402	$w(CH_2)_s(62) - \delta(CH_2)_s(12)$
		1237 (m)	1245	$t(CH_2)_s(78) - w(CH_2)_a(11)$
	Inactive	1130 (m)	1133	$r(CH_2)_s(48) + \nu(COC)_s(18)$
		1066 (m)	1069	$\nu(CC)(64) - \nu(COC)_s(18)$
		859 (w)	868	$\nu(COC)_s(39) - r(CH_2)_s(22)$
		271 (w)	274	$\delta(CCO)_s(27) + \delta(COC)(26)$
		216 (w)	215	$\delta(COC)(32) - \tau(CO)_s(22)$
$A_2(\parallel)$	1461 / 1454 (m)		1459	$\delta(CH_2)_a(95)$
	1342 (s)		1346	$w(CH_2)_a(85)$
	1240 (m)		1248	$t(CH_2)_a(84)$
	1103 (vs)	Inactive	1107	$\nu(COC)_a(77) - r(CH_2)_a(17)$
	958 (s)		965	$r(CH_2)_a(42) + \nu(COC)_a(23)$
	530 / 509 (w)		528	$\delta(CCO)_a(66) - r(CH_2)_a(21)$
	107 (m)		106	$\tau(CO)_a(99)$
$E_1(\perp)$	1466 (m)	1470 (sh)	1473	$\delta(CH_2)_s(76) + \nu(CC)(11)$
	1448 (w)	1447 (w)	1455	$\delta(CH_2)_a(91)$
	1411 (w)		1410	$w(CH_2)_s(65)$
	1358 (m)	1364 (m)	1360	$w(CH_2)_a(87)$
	1278 (m)	1283 (s)	1273	$t(CH_2)_s(63) - t(CH_2)_a(23)$
	1234 (w)	1237 (m)	1238	$t(CH_2)_a(56) + t(CH_2)_s(26)$
	1147 (s)	1147 (s)	1150	$r(CH_2)_s(21) + \nu(COC)_a(19)$
	1116 (vs)		1120	$\nu(COC)_s(44) - \nu(COC)_a(19)$
	1066 (m)	1064 (m)	1060	$\nu(CC)(35) + r(CH_2)_s(25)$
	947 (m)		949	$\nu(CC)(32) - \nu(COC)_a(15)$
	844 (s)	844 (s)	842	$r(CH_2)_a(33) + \nu(COC)_a(19)$
	532 (w)	534 (m)	525	$\delta(CCO)_a(34) + \delta(COC)(13)$
	363 (w)	358 (m)	351	$\delta(COC)(33) + \delta(CCO)_s(31)$
	217 (w)	216 (w)	219	$\delta(CCO)_s(37) + \delta(CCO)_a(18) - \tau(CC)(14)$
	166 (w)	160 (w)	166	$\tau(CC)(50) + \tau(CO)_a(27)$
			94	$\tau(CO)_s(52) + (CO)_a(31)$
		(b) Poly(ethylene-d_4 oxide)		
$A_2(\parallel)$	1117 (vs)		1120	$\nu(COC)_a(55) - w(CD_2)_a(34)$
	1089 (sh)		1090	$\delta(CH_2)_a(82)$
	996 (m)		989	$w(CD_2)_a(52) + \nu(COC)_a(29)$
	940(m)		939	$t(CD_2)_a(68) + r(CD_2)_a(28)$
	800 (m)		798	$r(CD_2)_a(28) - t(CD_2)_a(22) + \delta(CCO)_a(20)$
	453 (w)		443	$\delta(CCO)_a(52) - r(CD_2)_a(29)$
	95 (m)		98	$\tau(CO)_a(98)$
$E_1(\perp)$	1255 (m)		1253	$\nu(CC)(44) + w(CD_2)_s(31)$
	1145 (s)		1139	$\nu(COC)_a(36) + \delta(CD_2)_a(17)$
	1121 (s)		1109	$w(CD_2)_s(31) + \nu(COC)_s(23)$
	1087 (sh)		1075	$\delta(CD_2)_a(49) - \delta(CD_2)_s(17)$
	1050 (vw)		1047	$w(CD_2)_a(50) - \delta(CD_2)_s(24)$
	1016 (s)		1009	$\delta(CD_2)_a(31) - \nu(COC)_s(26)$
	942 (m)		940	$r(CD_2)_s(28) - t(CD_2)_a(24) + t(CD_2)_s(21)$
	919 (m)		910	$t(CD_2)_s(31) - \nu(CC)(22)$
	885 (vw)		868	$t(CD_2)_s(41) + t(CD_2)_s(27)$
	780 (w)		773	$w(CD_2)_s(43) - \nu(CC)(14)$
	703 (m)		691	$r(CD_2)_a(28) - t(CD_2)_a(18)$
	458 (w)		462	$\delta(CCO)_a(27) + \delta(COC)(17) - r(CD_2)_a(16)$
			305	$\delta(CCO)_s(30) + \delta(COC)(30)$
	183 (w)		186	$\delta(CCO)_s(45) + \delta(CCO)_a(17)$
	156 (m)		154	$\tau(CC)(68) + \tau(CO)_a(23)$
			85	$\tau(CO)_s(53) + \tau(CO)_a(29)$

[a] The signs denote the phase relations.

TABLE VI
CALCULATED VIBRATIONAL FREQUENCIES

Species	Calcd frequency, cm^{-1}	Assignment (Potential energy distribution, %)[a]
	(a) Threo-Diisotactic PEO-d_2 (A)	
A_2	1332	$\delta_a(66)$
	1247	$w_a(54) + t_a(25)$
	1113	$\nu_a(COC)(72)$
	968	$t_a(50) - w_a(26)$
	840	$r_a(50) + \delta_a(CCO)(17)$
E_1	1406	$w_s(47) + t_s(16)$
	1327	$\delta_a(69)$
	1310	$\delta_s(66) - t_s(14)$
	1261	$w_a(55) + t_a(25)$
	1107	$\nu_a(COC)(45) + \nu_s(COC)(26)$
	1084	$\nu(CC)(47) + r_s(18)$
	1074	$\nu_s(COC)(36) - \nu_a(COC)(12)$
	1010	$r_s(28) + t_s(26)$
	902	$t_a(30) + r_a(13)$
	793	$r_a(24) - w_s(23)$
	743	$r_a(25)$
	(b) Threo-Diisotactic PEO-d_2 (B)	
A_2	1340	$w_a(49) - t_a(29)$
	1294	$\delta_a(64) + w_a(20)$
	1085	$\nu_a(COC)(73)$
	998	$r_a(39) + t_a(24)$
	860	$t_a(34) + w_a(33)$
E_1	1351	$w_s(42) + \nu(CC)(21)$
	1331	$w_a(34) - \delta_s(22)$
	1319	$\delta_s(48) - w_s(13)$
	1293	$\delta_a(70) + w_a(14)$
	1169	$\nu_s(COC)(42) - t_s(30)$
	1080	$\nu_a(COC)(52)$
	1001	$\nu_s(COC)(36) + t_s(31)$
	959	$t_s(35) + w_a(18)$
	929	$r_s(38) + \nu(CC)(21)$
	873	$w_s(37) - \nu(CC)(24)$
	758	$r_a(24) + \nu_a(COC)(22)$
	(c) Threo-Disyndiotactic PEO-d_2	
A_2	1338	$w_{IIa}(41) - t_{IIa}(23)$
	1329	$\delta_{Ia}(59)$
	1294	$\delta_{IIa}(67) + w_{IIa}(19)$
	1254	$w_{Ia}(52) + t_{Ia}(25)$
	1106	$\nu_a(COC)_I(59) + w_{Ia}(18)$
	1078	$\nu_a(COC)_{II}(58) - \delta_a(CCO)_{II}(13)$
	974	$t_{IIa}(34) + r_{IIa}(18)$
	941	$t_{Ia}(46) - w_{Ia}(14)$
	847	$r_{Ia}(28) - t_{IIa}(19) - w_{IIa}(16)$
	730	$r_{Ia}(26) - r_{IIa}(16) - \nu_a(COC)_I(15)$
E_1	1407	$w_{Is}(46) + \nu_I(CC)(16) + t_{Is}(15)$
	1347	$w_{IIs}(32) + \nu_{II}(CC)(25) + \delta_{IIs}(19)$
	1337	$w_{IIa}(46) - t_{IIa}(26)$
	1328	$\delta_{Ia}(39) + w_{IIs}(22)$
	1320	$\delta_{IIs}(56) + \delta_{Ia}(12)$
	1312	$\delta_{Is}(61) - t_{Is}(13)$
	1293	$\delta_{IIa}(65) + w_{IIa}(18)$
	1256	$w_{Ia}(50) + t_{Ia}(23)$
	1169	$\nu_s(COC)_{II}(39) - t_{IIs}(32)$
	1106	$\nu(CC)_I(23) - \nu_s(COC)_I(18)$
	1100	$\nu_s(COC)_I(36) + w_{Ia}(15)$
	1087	$\nu_a(COC)_I(54) - \nu_a(COC)_{II}(19)$
	1075	$\nu_a(COC)_{II}(27) + \nu(CC)_I(24)$
	979	$\nu_s(COC)_{II}(18) - r_{Is}(17) + t_{IIs}(16)$
	971	$r_{Is}(12) + t_{IIs}(10)$
	965	$t_{IIa}(18) + t_{Ia}(14)$
	961	$t_{IIa}(15) + r_{IIs}(12) + r_{IIa}(12)$
	908	$\nu_{II}(CC)(30) - r_{Ia}(10)$
	861	$r_{IIs}(30) + w_{IIs}(25)$
	822	$w_{Is}(17) + w_{IIa}(15) + t_{IIa}(14)$
	768	$r_{Ia}(38) - \nu_s(COC)_I(17)$
	724	$\nu_a(COC)_I(13) + w_{Is}(12) + r_{IIa}(12)$
	(d) Erythro-Diisotactic PEO-d_2	
A	1376	$w_s(38) + \nu(CC)(23)$
	1327	$\delta_s(48)$
	1318	$\delta_a(46) - w_a(23)$
	1287	$w_a(30) + \delta_a(24)$
	1121	$\nu_a(COC)(29) + t_a(19)$
	1102	$\nu_a(COC)(34) - \nu_s(COC)(17)$
	1036	$\nu(CC)(34) + \nu_a(COC)(20)$
	956	$r_a(25) - t_s(20)$
	936	$t_a(18) - \nu_s(COC)(18)$
	856	$t_s(21) - w_a(19)$
	768	$r_s(26)$
E_1	1372	$w_s(43, 0°), \nu(CC)(19, 1°)$
	1327	$w_a(32, 0°), t_s(20, 0°)$
	1315	$\delta_s(43, 0°), \delta_a(30, 154°)$
	1287	$\delta_a(29, 0°), w_a(26, -6°)$
	1135	$\nu_a(COC)(20, 0°), \nu_s(COC)(18, 8°)$
	1101	$\nu_s(COC)(38, 0°), \nu_a(COC)(29, 139°)$
	1013	$\nu(CC)(37, 0°), r_s(18, 20°)$
	969	$t_a(24, 0°), t_s(16, 180°)$
	944	$t_s(21, 0°), r_s(21, 5°)$
	847	$w_s(22, 0°), r_a(17, -153°)$
	727	$r_a(23, 0°), w_s(18, -179°)$
	(e) Erythro-Disyndiotactic PEO-d_2	
A_2	1370	$w_{Ia}(29) + w_{IIa}(19) + \nu(CC)_a(17)$
	1332	$w_{IIa}(38) - \delta_{IIa}(24)$
	1316	$\delta_{Ia}(69)$
	1288	$\delta_{IIa}(30) - w_{Ia}(28)$
	1120	$\nu_a(COC)_{II}(49) + \nu(CC)_a(15)$
	1109	$\nu_a(COC)_I(70)$
	1025	$\nu_a(COC)_{II}(37) + t_{IIa}(24)$
	989	$\nu(CC)_a(39) + r_{IIa}(18)$
	878	$w_{IIa}(28) + r_{Ia}(20)$
	780	$w_{Ia}(21) - \nu(CC)_a(21) + r_{IIa}(14)$
E_1	1378	$w_{Ia}(21) + \delta_{IIa}(18) + \nu(CC)_a(16)$
	1368	$w_{IIs}(22) + \nu(CC)_s(19)$
	1331	$\delta_{IIs}(34) - w_{IIs}(26)$
	1323	$\delta_{Is}(26) - w_{IIa}(21)$
	1322	$\delta_{Is}(52) + w_{IIa}(11)$
	1318	$\delta_{Ia}(47) + w_{IIa}(16)$
	1285	$\delta_{IIa}(19) - w_{Ia}(18) + w_{Is}(17)$
	1283	$w_{Is}(26) - \delta_{IIs}(16)$
	1142	$\nu_s(COC)_{II}(36) - t_{IIa}(12)$
	1126	$\nu_a(COC)_{II}(43) + \nu(CC)_s(17)$
	1111	$\nu_a(COC)_I(68)$
	1071	$\nu_s(COC)_I(39) - \delta_s(CCO)_I(13)$
	1035	$\nu(CC)_a(40)$
	1026	$\nu_a(COC)_{II}(41) + t_{IIs}(20)$
	986	$\nu(CC)_s(37) - \delta_{Is}(11)$
	980	$t_{Ia}(37) + r_{Ia}(22)$
	936	$t_{Is}(39) + w_{Is}(19)$
	906	$t_{IIa}(26) + r_{IIa}(26)$
	878	$r_{Is}(34) + w_{IIs}(26)$
	810	$w_{IIa}(19) + r_{Ia}(17)$
	765	$\nu_s(COC)_{II}(23) - t_{Ia}(16) - w_{Ia}(15)$
	722	$r_{IIs}(29) - \nu_s(COC)_I(17)$

[a] For the E_1 species of erythro-diisotactic PEO-d_2, the phase relations in degrees are given.

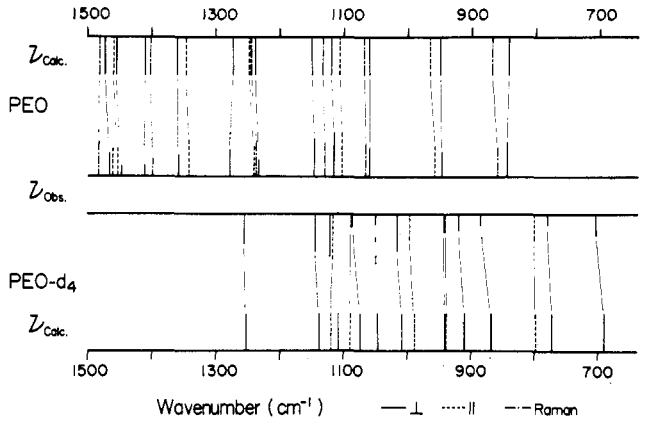

Figure 5. The observed and calculated frequencies for poly(ethylene oxide) and poly(ethylene-d_4 oxide). For the observed frequencies, solid lines, broken lines, and chain lines represent the perpendicular bands, parallel bands, and the Raman lines, respectively. For the calculated frequencies, solid lines represent the E_1 species, broken lines the A_2 species, and the chain lines the A_1 species.

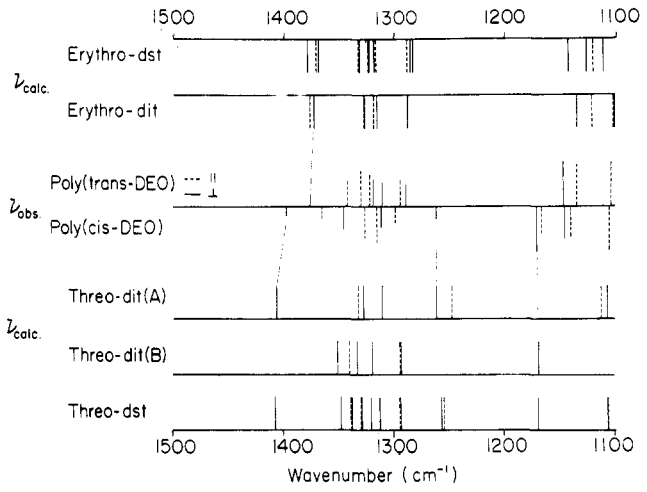

Figure 6. The observed frequencies for poly(*trans*-dideuterioethylene oxide) and poly(*cis*-dideuterioethylene oxide) (middle), and the calculated frequencies for the two erythro models (top) and the three threo models (bottom). The thin lines indicate the correspondence between the observed characteristic bands and the calculated frequencies.

vibrations), and the agreements between the calculated and observed frequencies in the 1500–650-cm^{-1} region (methylene bending and skeletal stretching) are especially good, giving maximum and average deviations of 1.92 and 0.50%, respectively, for both PEO and PEO-d_4. Thus, the set of force constants given in Table IV is considered to be sufficiently reliable for the present purpose.

The calculations of the normal modes for the five models based on the symmetry coordinates in the Appendix were carried out by using refined force constants. Here, the same local symmetry coordinates for the CH_2, CD_2, and CHD groups are used for simplicity. The calculated normal modes are given for the 1500–700-cm^{-1} region in Table VI and also are compared in Figure 6 for *trans*- and *cis*-PEO-d_2. For the observed frequencies, broken and solid lines represent the parallel and perpendicular bands, respectively. For the calculated frequencies, broken and solid lines represent the A (for the erythro-diisotactic model) or A_2 (for the other four models) and the E_1 species (for all the models), respectively.

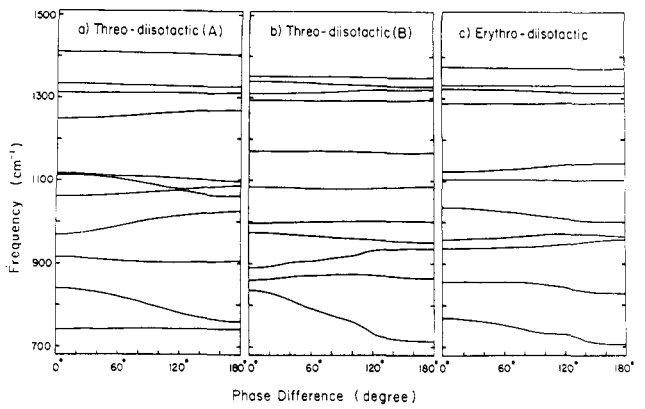

Figure 7. The frequency phase difference curves for (a) threo-diistactic (A), (b) threo-diisotactic (B), and (c) erythro-diisotactic poly(dideuterioethylene oxide) in the 1500–700-cm^{-1} region.

TABLE VII
INTERNAL COORDINATES[a]

Bond Lengths

$r_1[C_I–H_I]$, $r_1'[C_I–H_I']$, $r_2[C_{II}–H_{II}]$, $r_2'[C_{II}–H_{II}']$, $D_1[O(-1)–C_I]$, $D_2[C_{II}–O]$, $R[C_I–C_{II}]$

Bond Angles

$\omega_1[\angle H_IC_IO(-1)]$, $\omega_1'[\angle H_I'C_IO(-1)]$, $\phi_1[\angle H_IC_IC_{II}]$, $\phi_1'[\angle H_I'C_IC_{II}]$, $\omega_2[\angle H_{II}C_{II}O]$, $\omega_2'[\angle H_{II}'C_{II}O]$, $\phi_2[H_{II}C_{II}C_I]$, $\phi_2'[\angle H_{II}'C_{II}O]$, $\delta_1[\angle H_IC_IH_I']$, $\delta_2[\angle H_{II}C_{II}H_{II}']$, $\Theta_1[\angle O(-1)C_IC_{II}]$, $\Theta_2[\angle C_IC_{II}O]$, $\theta[\angle C_{II}OC_I(+1)]$

Internal Rotation Angles

$T_1[\angle C_{II}(-1)O(-1)C_IC_{II}]$, $T_2[\angle C_IC_{II}OC_I(+1)]$, $\tau[\angle O(-1)C_IC_{II}O]$

[a] Numbering of atoms is shown below.

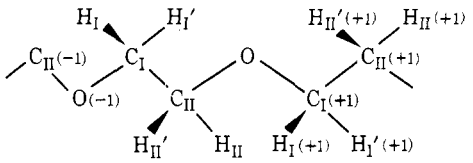

Discussion

The distinct 1169-cm^{-1} band characteristic of the cis polymer corresponds only to the calculated modes of the threo-diisotactic B and threo-disyndiotactic models. Two bands at 1261 and 1397 cm^{-1} of the cis polymer correspond to the modes calculated for the threo-diisotactic A and threo-disyndiotactic models. The 1376-cm^{-1} band of the trans polymer corresponds only to the calculated frequencies of the erythro models. In this way the characteristic bands of the cis polymer in this region can be clearly assigned to the modes of the threo models, and those of the trans polymer to the erythro models. Such a correspondence seems to be far more reasonable than the reverse one. The intensity and dichroism of the four bands mentioned above can be reasonably interpreted by the potential energy distributions given in Table VI. The strong perpendicular band at 1169 cm^{-1} of the cis polymer is assigned to the E_1 mode including ν_s(COC) (42%) and t_s (CHD) (30%), which should be strong and perpendicularly polarized. The 1267- and 1390-cm^{-1} bands of the cis polymer and the 1376-cm^{-1} band of the trans polymer are all weak and perpendicular. These three bands are assigned to the E_1 modes consisting of the couplings of w(CHD), t(CHD), and/or ν(CC). No appreciable contributions of the polar groups are found in these bands.

TABLE VIII
LOCAL SYMMETRY COORDINATES FOR THE jTH MONOMERIC UNIT

$$(j) = \begin{vmatrix} \mathbf{s}_1(j) \\ \mathbf{s}_2(j) \\ \mathbf{s}_3(j) \\ \mathbf{s}_4(j) \end{vmatrix}$$

$\mathbf{s}_1(j) =$	$s_1 = (1/\sqrt{2})\Delta(r_1 + r_1')$	$\nu_s(CH_2)$
	$s_2 = (1/\sqrt{2})\Delta(r_1 - r_1')$	$\nu_a(CH_2)$
	$s_3 = (1/\sqrt{20})\Delta(4\delta_1 - \omega_1 - \omega_1' - \phi_1 - \phi_1')$	$\delta(CH_2)$
	$s_4 = (1/2)\Delta(\omega_1 + \omega_1' - \phi_1 - \phi_1')$	$w(CH_2)$
	$s_5 = (1/2)\Delta(\omega_1 - \omega_1' - \phi_1 + \phi_1')$	$t(CH_2)$
	$s_6 = (1/2)\Delta(\omega_1 - \omega_1' + \phi_1 - \phi_1')$	$r(CH_2)$
	$s_7 = \Delta D_1$	$\nu(CO)$
	$s_8 = (1/\sqrt{30})\Delta(5\Theta_1 - \delta_1 - \omega_1 - \omega_1' - \phi_1 - \phi_1')$	$\delta(CCO)$
	$s_9 = \Delta T_1$	$\tau(CO)$
	$s_{red} = (1/\sqrt{6})\Delta(\Theta_1 + \delta_1 + \omega_1 + \omega_1' + \phi_1 + \phi_1')$	Redundant coordinate
$\mathbf{s}_2(j) =$	$s_{10} = (1/\sqrt{2})\Delta(r_2 + r_2')$	$\nu_s(CH_2)$
	$s_{11} = (1/\sqrt{2})\Delta(r_2 - r_2')$	$\nu_a(CH_2)$
	$s_{12} = (1/\sqrt{20})\Delta(4\delta_2 - \omega_2 - \omega_2' - \phi_2 - \phi_2')$	$\delta(CH_2)$
	$s_{13} = (1/2)\Delta(\omega_2 + \omega_2' - \phi_2 - \phi_2')$	$w(CH_2)$
	$s_{14} = (1/2)\Delta(\omega_2 - \omega_2' - \phi_2 + \phi_2')$	$t(CH_2)$
	$s_{15} = (1/2)\Delta(\omega_2 - \omega_2' + \phi_2 - \phi_2')$	$r(CH_2)$
	$s_{16} = \Delta D_2$	$\nu(CO)$
	$s_{17} = (1/\sqrt{30})\Delta(5\Theta_2 - \delta_2 - \omega_2 - \omega_2' - \phi_2 - \phi_2')$	$\delta(CCO)$
	$s_{18} = \Delta T_2$	$\tau(CO)$
	$s_{red} = (1/\sqrt{6})\Delta(\Theta_2 + \delta_2 + \omega_2 + \omega_2' + \phi_2 + \phi_2')$	Redundant coordinate
$\mathbf{s}_3(i) =$	$s_{19} = \Delta R$	$\nu(CC)$
	$s_{20} = \Delta\tau$	$\tau(CC)$
$\mathbf{s}_4(j) =$	$s_{21} = \Delta\theta$	$\delta(COC)$

TABLE IX
INTERMEDIATE SYMMETRY COORDINATES FOR THE pTH ASYMMETRIC UNIT

(a) PEO, PEO-d_4, and Diisotactic PEO-d_2

$$\mathbf{S}(p) = \begin{vmatrix} \mathbf{S}(p)_s \\ \mathbf{S}(p)_a \end{vmatrix}$$

$$\mathbf{S}(p)_s = \begin{vmatrix} (1/\sqrt{2})[\mathbf{s}_1(j) + \mathbf{s}_2(j)] \\ \mathbf{s}_3(j) \\ \mathbf{s}_4(j) \end{vmatrix}$$

$$\mathbf{S}(p)_a = \begin{vmatrix} (1/\sqrt{2})[\mathbf{s}_1(j) - \mathbf{s}_2(j)] \end{vmatrix}$$

(b) Threo-Disyndiotactic PEO-d_2

$$\mathbf{S}(p) = \begin{vmatrix} \mathbf{S}(p)_{Is} \\ \mathbf{S}(p)_{IIs} \\ \mathbf{S}(p)_{Ia} \\ \mathbf{S}(p)_{IIa} \end{vmatrix}$$

$$\mathbf{S}(p)_{Is} = \begin{vmatrix} (1/\sqrt{2})[\mathbf{s}_1(i) + \mathbf{s}_2(j)] \\ \mathbf{s}_3(j) \end{vmatrix}$$

$$\mathbf{S}(p)_{IIs} = \begin{vmatrix} (1/\sqrt{2})[\mathbf{s}_1(j+1) + \mathbf{s}_2(j+1)] \\ \mathbf{s}_3(j+1) \\ (1/\sqrt{2})[\mathbf{s}_4(j) + \mathbf{s}_4(j+1)] \end{vmatrix}$$

$$\mathbf{S}(p)_{Ia} = \begin{vmatrix} (1/\sqrt{2})[\mathbf{s}_1(j) - \mathbf{s}_2(j)] \end{vmatrix}$$

$$\mathbf{S}(p)_{IIa} = \begin{vmatrix} (1/\sqrt{2})[\mathbf{s}_1(j+1) - \mathbf{s}_2(j+1)] \\ (1/\sqrt{2})[\mathbf{s}_4(j+1) - \mathbf{s}_4(j+1)] \end{vmatrix}$$

(c) Erythro-Disyndiotactic PEO-d_2

$$\mathbf{S}(p) = \begin{vmatrix} \mathbf{S}(p)_{Is} \\ \mathbf{S}(p)_{IIs} \\ \mathbf{S}(p)_{Ia} \\ \mathbf{S}(p)_{IIa} \end{vmatrix}$$

$$\mathbf{S}(p)_{Is} = \begin{vmatrix} (1/\sqrt{2})[\mathbf{s}_2(j) + \mathbf{s}_1(j+1)] \\ \mathbf{s}_4(j) \\ (1/\sqrt{2})[\mathbf{s}_3(j) + \mathbf{s}_3(j+1)] \end{vmatrix}$$

$$\mathbf{S}(p)_{IIs} = \begin{vmatrix} (1/\sqrt{2})[\mathbf{s}_1(j) + \mathbf{s}_2(j+1)] \\ \mathbf{s}_4(j+1) \end{vmatrix}$$

$$\mathbf{S}(p)_{Ia} = \begin{vmatrix} (1/\sqrt{2})[\mathbf{s}_2(j) + \mathbf{s}_1(j+1)] \\ (1/\sqrt{2})[\mathbf{s}_3(j) - \mathbf{s}_3(j+1)] \end{vmatrix}$$

$$\mathbf{S}(p)_{IIa} = \begin{vmatrix} (1/\sqrt{2})[\mathbf{s}_1(j) - \mathbf{s}_2(j+1)] \end{vmatrix}$$

In the region lower than 1100 cm^{-1}, several distinct spectral differences are also found between two polymers. As shown in Figure 7 the frequency–phase difference curves for this region (lower than 1100 cm^{-1}) reveal rather complicated behaviors, while those in the region higher than 1100 cm^{-1} are almost flat. This fact supports the experimental argument that the vibrational modes with frequencies at 1500–1100 cm^{-1} localize mainly in the monomeric unit, and it may be suitable to examine the spectral bands in this region for the present purpose. Thus it may be concluded that the cis polymer corresponds to the threo models and the trans polymer to the erythro models.

This correspondence leads to the inversion ring opening in the polymerization of ethylene oxide. In the case of 2-butene oxide, Vandenberg first reported the inversion ring opening from the results of polymerization of trans (optically active) and cis (meso) monomers with cationic catalysts, *i.e.*, Al(i-Bu)$_3$–H_2O and $AlEt_3$–H_2O–acetylacetone–l-menthol, re-

spectively.[6] Barlow confirmed this type of opening by X-ray analysis of poly(*trans*-2-butene oxide) which was found to be erythro diisotactic.[7] Present work on PEO shows that the conclusion about inversion ring opening may be extended to more general cases, that is, various types of polymerizations with cationic, anionic, and coordination catalysts.

Appendix

The internal coordinates and the numbering of the atoms are given in Table VII. The local symmetry coordinates for the jth monomeric unit, and the intermediate symmetry coordinates for the pth asymmetric unit (corresponding to eq 7 of ref 8) are given in Tables VIII and IX, respectively.

In Table IX, the subscripts s and a represent symmetric and antisymmetric with respect to the twofold axes (on the midpoint of the C–C bond or the oxygen atom), respectively. The subscripts I and II for threo-disyndiotactic PEO-d_2 refer to the twofold rotation axes on the C–C bonds of the Newman projections I and II, respectively. The definition of the

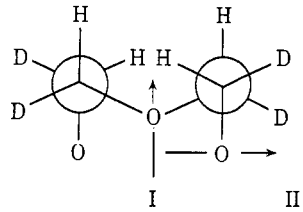

subscripts I and II for erythro-disyndiotactic PEO-d_2 are different from the threo-disyndiotactic case. These are associated with the twofold rotation axes on the oxygen atoms shown by the following Newman projection.

(6) E. J. Vandenberg, *J. Amer. Chem. Soc.*, **83**, 3538 (1961); *J. Polym. Sci., Part B*, **2**, 1085 (1964).
(7) M. Barlow, *J. Polym. Sci., Part A-2*, **4**, 121 (1966).
(8) H. Tadokoro, M. Kobayashi, Y. Kawaguchi, A. Kobayashi, and S. Murahashi, *J. Chem. Phys.*, **38**, 703 (1963).

Thermodynamics of Equilibrium Copolymerization in Solution. A General Expression and Its Application to Bulk Copolymerization

P. E. Harvey and J. Leonard*

Département de Chimie, Université Laval, Quebec 10, Canada.
Received June 16, 1972

ABSTRACT: Reversible addition of monomer A and monomer B to active copolymer chains leading to the formation of A–A, A–B, B–B, and B–A bonds is considered. P_{AA}, the probability that monomer A is added to a chain ending with A unit, is set equal to $K\exp(-\Delta G_{AAs}/RT)$, where K is a numerical constant found to be one and ΔG_{AAs} is the free energy change upon the addition in solution under conditions prevailing at equilibrium of 1 mol of monomer A to copolymer chains in order to form A–A bonds. All other probability terms P_{AB}, P_{BB}, and P_{BA} are defined analogously, and a simple general expression written in terms of free energy of polymerization in solution is obtained. This general expression is applied to equilibrium bulk copolymerization where monomers A and B are solvent for their copolymer. Making allowance for the nonideal behavior of the solution through the use of Flory's expression for the partial molar free energy of mixing of monomers and copolymer, an equation is written in terms of volume fractions of monomer A, ϕ_a, monomer B, ϕ_b, and copolymer, ϕ_p. Variations of ϕ_a and ϕ_b with ϕ_p and that of x_a with ϕ_a^0 are computed for different values of free energy of polymerization and interaction parameters between monomer molecules, x_a being the mole fraction of monomer A in the copolymer and ϕ_a^0 the volume fraction of the same monomer in the initial feed.

In recent years, copolymerization with depropagation with respect to both monomers has been treated by a number of authors. Solution to this complex problem has been considered through a kinetic[1-3] as well as thermodynamic approach.[4-6] Thermodynamic treatments by Theil[4] and Sawada[5] seem to refer to the formation of pure copolymer without any reference to the medium of copolymerization. More recently, Izu and O'Driscoll[6] have considered complete reversibility for copolymerization in an ideal solution and made use of a Monte Carlo technique for a numerical solution.[7] In the present paper, complete reversibility in equilibrium copolymerization in solution is considered, taking into account the nonideal behavior of the medium. Specific equations for equilibrium bulk copolymerization where monomers are solvent for their copolymer are derived.

The Model

In the case of equilibrium copolymerization in solution with complete reversibility, the overall equilibrium is established with respect to four reversible reactions

$$\sim A^* + A \rightleftharpoons \sim AA^* \quad (I)$$

$$\sim B^* + A \rightleftharpoons \sim BA^* \quad (II)$$

$$\sim B^* + B \rightleftharpoons \sim BB^* \quad (III)$$

$$\sim A^* + B \rightleftharpoons \sim AB^* \quad (IV)$$

These equations describe the reversible addition of monomers A and B to active chains ending with A* or B*; this set of reactions is known as the dyad model.[3]

In the present work, we consider the formation of 1 base mol of copolymer of infinite molecular weight and of composition

(1) A. A. Durgaryan, *Vysokomol. Soedin.*, **8**, 790 (1966).
(2) J. E. Hazell and K. J. Ivin, *Trans. Faraday Soc.*, **58**, 342 (1962); **61**, 2330 (1965).
(3) J. A. Howell, M. Izu, and K. F. O'Driscoll, *J. Polym. Sci., Part A-1*, **8**, 699 (1970).
(4) M. H. Theil, *Macromolecules*, **2**, 137 (1969).
(5) H. Sawada, *J. Polym. Sci., Part A-1*, **5**, 1383 (1967).
(6) M. Izu and K. F. O'Driscoll, *Polym. J.*, **1**, 27 (1970).
(7) M. Izu and K. F. O'Driscoll, *J. Polym. Sci., Part A-1*, **8**, 1675 (1970).